

# Ostwald's Rule of Stages and Its Role in CdSe Quantum Dot Crystallization

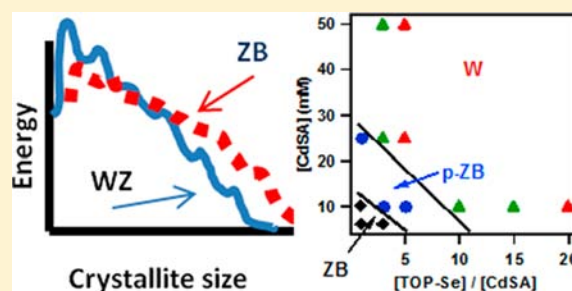
Aaron L. Washington, II,<sup>†</sup> Megan E. Foley,<sup>†</sup> Soshan Cheong,<sup>‡,§</sup> Lieth Quffa,<sup>†</sup> Christopher J. Breshike,<sup>†</sup> John Watt,<sup>‡</sup> Richard D. Tilley,<sup>‡</sup> and Geoffrey F. Strouse<sup>\*,†</sup>

<sup>†</sup>Department of Chemistry and Biochemistry, Florida State University, Tallahassee, Florida 32306-4390, United States

<sup>‡</sup>School of Chemical Physical Sciences, The MacDiarmid Institute for Advanced Materials and Nanotechnology, Victoria University of Wellington, New Zealand

**S** Supporting Information

**ABSTRACT:** A century ago Ostwald described the “Rule of Stages” after deducing that crystal formation must occur through a series of intermediate crystallographic phases prior to formation of the final thermodynamically stable structure. Direct evidence of the Rule of Stages is lacking, and the theory has not been implemented to allow isolation of a selected structural phase. Here we report the role of Ostwald's Rule of Stages in the growth of CdSe quantum dots (QDs) from molecular precursors in the presence of hexadecylamine. It is observed that, by controlling the rate of growth through the reaction stoichiometry and therefore the probability of ion-packing errors in the growing QD, the initially formed zinc blende (ZB) critical nuclei representing the kinetic phase can be maintained at sizes >14 nm in diameter without phase transformation to the thermodynamic wurtzite (WZ) structure. An intermediate pseudo-ZB structure is observed to appear at intermediate reaction conditions, as predicted by Ostwald. The ZB and pseudo-ZB structures convert to the WZ lattice above a critical melting temperature. This study validates Ostwald's Rule of Stages and provides a phase diagram for growth of CdSe QDs exhibiting a specific crystallographic motif.



## INTRODUCTION

Formation of a specific crystal morphology, whether at the nanoscale or in the bulk, is governed by classical nucleation and crystal growth theories.<sup>1–3</sup> While the growth mechanism for a crystal is well known, the initially formed structure at the point of nucleation is poorly understood. Ostwald's “Rule of Stages” predicts nucleation will occur with the formation of a critical nucleus having the lowest surface energy.<sup>4–6</sup> The importance of surface energy for polymorph isolation has been reported, and typically the kinetic structure is more stable at small crystallite size.<sup>7–10</sup> As the crystallite grows the crystal structure will continuously change, reflecting the most stable polymorph for a given size until a phase transition to the thermodynamic phase occurs at the point the lattice energy exceeds the energy difference between the metastable and thermodynamic phases. Evidence for the Rule of Stages has been inferred, but only recently have Ostwald's empirical rules been actively investigated in materials. Metal chalcogenide semiconductors offer a unique opportunity to explore the importance of Ostwald's Rule of Stages for quantum dot (QD) growth due to the ubiquitous knowledge about the growth of metal chalcogenide QDs from molecular precursors, which is influenced by the interplay of surface energy,<sup>11</sup> monomer activity,<sup>12</sup> and growth rate.<sup>13,14</sup> Since QDs are a technologically important material<sup>15–22</sup> in which the selective isolation of a specific crystallographic phase in CdSe can influence future technology design,

understanding the growth and the ability to control phases is an important step. For instance, the formation of cubic nuclei followed by rapid growth of wurtzite (WZ) arms on CdSe tetrapods has been observed.<sup>23</sup> In core–shell, multishell, or doped magnetic semiconductors the formation of a cubic core for CdSe can enhance the ability to grow a controlled core–shell architecture<sup>24</sup> or even lead to enhanced ion doping.<sup>25</sup> Regardless of the intended application, systematic control of the structure at the point of nucleation is crucial.

Ostwald's Rule of Stages predicts that the initially nucleated structure in the quintessential metal chalcogenide, namely CdSe, should be zinc blende (ZB) due to a lower surface energy, even though the WZ structure is thermodynamically favored and the only structure reported in bulk crystals. In CdSe thin films<sup>26</sup> and QDs<sup>27</sup> the isolated crystal phase was postulated to depend on reaction conditions, with high monomer concentration favoring the ZB phase and low monomer concentration favoring the WZ phase. As the critical nuclei grow, a relaxation to the thermodynamic structure occurs via a phase transition. Although CdSe QDs have been reported to be isolated in the ZB and WZ phases, the rationale for which structure will form and why is still debated.<sup>28–30</sup> Ostwald's Rule of Stages can offer an explanation for the reported observations

Received: March 27, 2012

Published: August 24, 2012

and, more importantly, a rational approach to selectively isolate the structure of choice, whether kinetic (cubic) or thermodynamic (WZ), by controlling the growth conditions.

In this article Ostwald's Rule of Stages is used to control the structure isolated from a QD growth process, allowing the selective isolation of CdSe QDs of 2–14 nm in diameter with the ZB structure, the WZ structure, or a phase with a high density of stacking faults, which we identify as a pseudo-zinc blende (pseudo-ZB) structure. Control of the structure is achieved by merely controlling the reactant concentrations. With control of the reaction monomer concentration, the rate of QD growth following nucleation is influenced, allowing the initially nucleated ZB structure in accord with Ostwald's Rule of Stages to be maintained well past the point previously reported. The results demonstrate that the initial nucleation event occurs in the lowest energy structure, which is the kinetic phase, which will remain in the ZB kinetic phase up to 14 nm in size without structural relaxation due to low defect densities and epitaxial ion addition. If growth rates are rapid, as observed at high monomer concentrations, stacking faults are formed during QD growth, which results in a low-temperature thermal relaxation to the WZ structure early in the growth process, with suppression of the melting points between crystallographic phases as the concentration of defects within a crystal lattice increases. The observation of a stable ZB structure under identical reaction conditions (ligand, temperature, time) indicates that Ostwald's empirical prediction of the Rule of Stages is valid for QD nucleation and growth processes. The study is limited to sizes above 2 nm since the critical nuclei for CdSe are believed to be on the order of  $\sim 1.5$  nm (180 CdSe units).<sup>31,32</sup> Controlled nucleation and growth under systematic reaction conditions demonstrate that Ostwald's Rule of Stages is followed in QD growth, allowing a detailed binary phase diagram for CdSe to be developed for the routine isolation of a desired phase over a wide size regime (2–14 nm). The ZB and WZ samples exhibit no time-dependent conversion during lyothermal growth, whereas the pseudo-ZB phase readily converts to a WZ structure after 24 h post-synthesis annealing under solvothermal conditions due to the annealing of structural inclusions in the QD. As anticipated, the ZB structure exhibits a first-order phase transition at  $\sim 380$  °C in the solid state with formation of the WZ phase. The development of a simple binary phase diagram that does not require structural directing ligands, exhibits phase stability, and conforms to the rules of crystal growth provides a new approach to reaction design, particularly when targeting metastable phases in nanoscale materials. For applications of QDs, understanding the rules that govern structural control may allow more complex hetero-structured materials and architectural shapes (i.e., tetrapod, rod, plates, sphere) to be rationally designed at the synthetic level rather than accidentally produced.

## ■ EXPERIMENTAL SECTION

**Chemicals.** All reactants and solvents were used without further purification. Cadmium stearate (CdSA, 90%) and selenium powder (Se, 99.99%) were both purchased from Strem Chemicals. Tri-*n*-octylphosphine (TOP, 90%) was purchased from Alfa Aesar. Octadecene, hexadecylamine (HDA), and decane were purchased from Acros Organics.

**Reaction Conditions for Formation of CdSe QDs.** Spherical CdSe QDs from 2 to 14 nm in diameter were prepared by previously described hot-injection lyothermal routes at 220 °C using CdSA and trioctylphosphine selenide (TOP-Se) as monomers in the presence of

hexadecylamine (HDA) as a capping agent.<sup>33</sup> The selected QD samples reported herein were isolated by withdrawal of an aliquot of the reaction mixture during growth and cooled to 60 °C prior to precipitation by addition of methanol (MeOH). The precipitate was centrifuged and re-dissolved in toluene, followed by a second precipitation step to remove excess ligand and monomer. The reaction conditions that generate the phase diagram are applicable to both hot injection and microwave-enhanced methods. In this article, only the hot injection (lyothermal) method is shown in the figures in order to generalize the results to a broader community.

The binary phase diagram is generated by carrying out the reactions at 1 M HDA, 1 M TOP-Se, and CdSA concentrations of 6, 10, 12.5, 25, and 50 mM. Control over the isolated crystal phase reflects changes in the monomer concentration and metal-to-chalcogenide mole ratios *only*. Although the Cd:Se mole ratio was varied to generate the phase diagram, the fully characterized QDs illustrated in herein represent QDs grown using a 1:5 Cd:Se mole ratio for the WZ samples, 1:1 for the ZB structure, and 1:3 for the pseudo-ZB phase.

**Growth Kinetics.** The growth kinetics and nuclei concentration for QD reactions at 170 °C were evaluated using 1:1, 1:5, and 1:15 Cd:Se mole ratios. The changes in QD size and concentration were monitored by analysis of the UV–vis spectra for 0.5 mL aliquots diluted to 10 mL in toluene sampled every 30 s. The change in size with time was plotted on the basis of the position of the first exciton transition, while the number of nuclei was extracted by conversion of the absorption intensity to a concentration using Beer–Lambert law analysis based upon the size-dependent extinction coefficients for CdSe QDs.<sup>34</sup>

**Characterization.** QD size, shape, and structure were determined by a combination of powder X-ray diffraction (pXRD), transmission electron microscopy (TEM), selected area electron diffraction (SAED), and absorption spectroscopy. Room-temperature pXRD spectra were recorded on 10 mg powdered samples on a Rigaku DMAX 300 Ultima III powder X-ray diffractometer (using Cu  $K\alpha$  radiation,  $\lambda = 1.5418$  Å). The pXRD was calibrated to Si. TEM and SAED were obtained using a JEOL 2010 instrument operated at an acceleration voltage of 200 keV. TEM samples were prepared as dilute solutions in toluene. One drop of the prepared solution was placed onto a holey carbon 400 mesh TEM grid and allowed to evaporate under ambient conditions. The  $d$ -spacing for the observable diffraction rings was analyzed by calibration from the diffraction pattern of gold nanocrystals.

Structural assignments from SAED and pXRD are based on indexing to the patterns for ZB,  $F43m$ , and WZ,  $P63mc$ . The ZB structure is assigned for materials that exhibit well-defined reflections corresponding to the (111), (200), (311), and (220) reflections in the ZB phase. The WZ phase is assigned to samples that exhibit three definable features in the 40–60° region corresponding to the (110), (103), and a combination of the (200), (112), and (201) reflections. The appearance of the characteristic (103) and loss of the ZB (200) reflection are mainly used to distinguish between a pure WZ assignment and a system containing stacking faults, which is referred to as the pseudo-ZB phase herein.

All optical experiments were performed on  $1 \times 10^{-9}$  M CdSe QDs dissolved in toluene. Absorption measurements were performed on a Varian Cary 50 UV–vis spectrophotometer. Photoluminescence measurements were performed on a Varian Cary Eclipse fluorescence spectrophotometer.

## ■ RESULTS AND DISCUSSION

Reactions carried out as a function of reaction time at identical reaction temperature (220 °C) and reaction additives (HDA), but at various CdSA concentrations and Cd:Se monomer ratios, were observed to produce a distinct population of crystallite phases within defined reaction boundaries. In Figure 1A, the observed change in the pXRD pattern for reactions carried out at various CdSA concentrations from 6 to 200 mM at a 3:1 CdSA:TOP-Se monomer ratio is shown. As the concentration

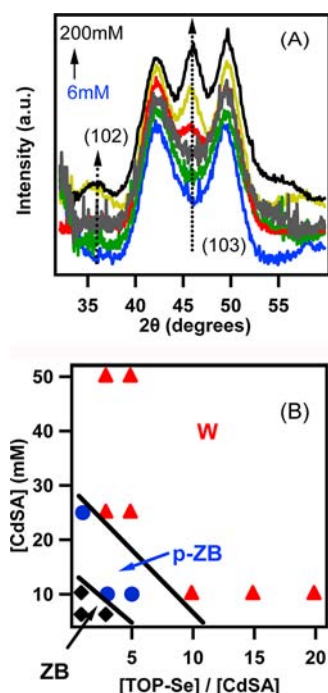


**Figure 1.** (A) pXRD data for reactions carried out at 220 °C at 3:1 TOP-Se: CdSA with concentrations of CdSA from 6 to 200 mM. (B) Binary phase diagram for the reaction conditions that allow isolation of the ZB (black diamond), pseudo-ZB (blue circle), and WZ (red triangle) crystal phases in CdSe QDs. The points represent CdSe QDs grown between 2 and 14 nm in diameter under the various reaction conditions.

of monomer increases, the pXRD exhibits a change from ZB to WZ based upon a qualitative pattern analysis. Similar behavior is observed with a conversion from ZB to WZ with increasing TOP-Se: CdSA monomer ratio at a fixed CdSA concentration (Figures SI-1–SI-3). Inspection of the pXRD patterns at various reaction conditions allows a tentative assignment of phase boundaries for specific reaction conditions, which can be presented as a binary phase diagram (Figure 1). The binary phase diagram is generated from multiple reactions producing QDs between 2 and 14 nm in diameter grown at Cd-to-Se mole ratios of 1:1 to 1: 20 with CdSA concentrations between 2 and 50 mM.

The structure assignments reported in Figure 1 are based primarily upon analysis of the pXRD data (Figures 2 and SI-1–SI-3) and verified by analysis of selected TEM-SAED data (Figures 3 and SI-4–SI-7). The diagram is reproducible for both lyothermal and microwave-based synthetic methods. Due to the number of CdSe QDs prepared to generate the phase diagram, only selected TEM, TEM-SAED, and pXRD analytical data are shown.

The isolated QDs are sized using TEM, absorption spectra, and pXRD Scherrer broadening analysis. It is important to note that the width of the features in the pXRD can obscure structural assignments due to the overlap of the diffraction features. In addition, the limited number of lattice planes within a QD results in peak broadening since constructive/destructive interference by Bragg's law is not adequate to produce sharp features. Other broadening effects in the pXRD arise from strain and stacking faults within the dot. TEM analysis of size is more accurate, therefore, than pXRD sizing.

All isolated QDs are observed to be spherical with narrow size dispersities based upon absorption peak width analysis and inspection of the TEM spectra. Size dispersity and shape analysis was carried out by low-resolution TEM on QDs grown to ~3.0 nm in size prior to isolation under reaction conditions of 1:1, 1:5, and 1:15 Cd:Se (Figures SI-1–SI-3, respectively). The pXRD data exhibit ZB- and WZ-type patterns depending on reaction conditions.

The structural boundaries can be analyzed by inspection of the high-resolution TEM and TEM-SAED data for ~5.0 nm QDs shown in Figure 3, where ZB ( $5.0 \pm 0.7$  nm) is isolated at 1:1 Cd:Se at 10 mM CdSA and WZ ( $5.0 \pm 0.8$  nm) at 1:15 Cd:Se at 10 mM CdSA. The size dispersity plots for Figure 3 are included in Figure SI-8. Additional TEM data on 14 nm ZB CdSe (1:1 Cd:Se) and 18 nm WZ CdSe (1:15 Cd:Se) are reported in Figure SI-7. TEM images of pseudo-ZB CdSe QDs of  $8.0 \pm 0.6$  nm (Figure SI-9) and 30 nm (Figure SI-6) are presented in the Supporting Information. The TEM images for pseudo-ZB QDs exhibit stacking faults. The size dispersities for all QDs are calculated from QDs isolated from the raw reaction without size selection, and a plot of size vs frequency is generated from analyzing >200 QDs. The reported QD size range represents the base width of a Gaussian fit.

In the binary phase diagram (Figure 1B), three structural regimes are identifiable for different monomer conditions. At high mole ratios of the monomers (Se: Cd > 10:1) or high Cd precursor concentration (>30 mM in Cd), the WZ lattice is exclusively isolated from the reaction and can be indexed to  $P63mc$ , standard card no. 186 (Figure 2vi–x). At low monomer mole ratios (Se: Cd < 5:1) or low Cd precursor concentration (<10 mM in Cd), the ZB phase is selectively isolated and can be indexed to  $F4_3m$ , standard card no. 216 (Figure 2i–v). In Figure 2A, the pXRD features between 20° and 80° ( $2\theta$ ) for selected samples from the ZB CdSe QDs of sizes (i) 5.2, (ii) 8.9, (iii) 9.6, (iv) 12.9, and (v) 14.3 nm are indexed to the (111), (220), (311), (400), and (331) planes of the ZB structure. In Figure 2B, the pXRD patterns of WZ CdSe QDs of sizes (vi) 5.0, (vii) 7.2, (viii) 8.6, (ix) 9.6, and (x) 10.7 nm are indexed to the (100), (002), (101), (102) (broadened in 5.0 nm sample), (110), and (103) (unresolved in 5.0 nm sample) planes and show a diffraction feature attributed to the combination of the (200), (112), and (201) reflections. Higher order diffraction features between 60° and 80° can be assigned as the QD size increases, indicative of highly crystalline QDs. The phase assignments for the isolated ZB and WZ crystal phases from pXRD are confirmed by inspection of the SAED patterns in Figure 3 (Figures SI-4 and SI-5). The ZB sample exhibits clearly defined (111), (220), (311), and (400) diffraction rings and lacks any intensity assignable to the WZ structure. The SAED pattern for the WZ sample exhibits a clear diffraction pattern which can be indexed to a WZ structural motif, confirming the structure assignments from the pXRD patterns in Figure 2.

QDs grown under the reaction conditions for the pseudo-ZB phase appear to be isolable as a WZ on the basis of the pXRD pattern but exhibit WZ and ZB reflections in the TEM-SAED pattern (Figure SI-6). pXRD data for a time-dependent growth at 1:5 Cd:Se (10 mM CdSA) exhibit a size-dependent pXRD pattern (Figure SI-10). The pattern is assignable to ZB at small sizes (i, ii) and appears to be consistent with WZ (iii, iv) at the largest size. The pseudo-ZB phase is assigned on the basis of the appearance of the WZ (102) in samples iv and v, the peak positions of the WZ (110) and WZ (112) in samples i–v, and

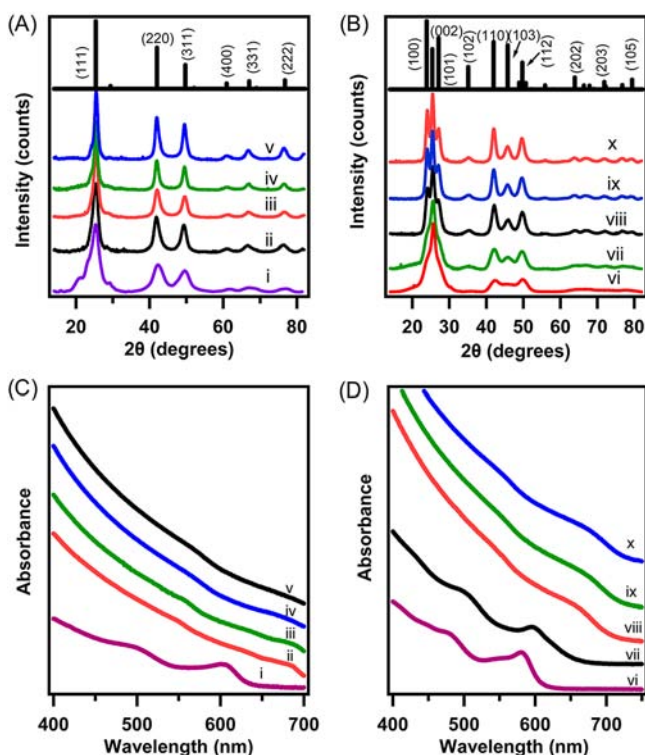


**Figure 2.** Isolated CdSe QDs in (A) kinetic zinc blende (ZB) and (B) thermodynamic wurtzite (WZ) structural phases. (A) The pXRD and (C) optical absorption of the ZB phase for (i) 5.2, (ii) 8.9, (iii) 9.6, (iv) 12.9, and (v) 14.3 nm CdSe. In addition, a TEM image and SAED pattern for sample iii are shown in Figures SI-3 and SI-4. (B) The pXRD and optical absorption of the WZ phase for (vi) 5.0, (vii) 7.2, (viii) 8.6, (ix) 9.6, and (x) 10.7 nm CdSe. The SAED patterns for samples v and x are shown in Figure SI-3.

the clear presence of the ZB (311) in samples i–iii. The presence of stacking faults in the TEM images in Figures SI-6 and SI-9 for the pseudo-ZB structures explains the apparent discrepancy, since stacking faults can lead to mis-assignment of the pXRD pattern for CdSe QDs. In fact, the presence of as few as *two* ZB stacking faults in an otherwise WZ nanocrystal has been postulated to lead to the observation of a ZB pXRD pattern due to loss of the (103) reflection intensity based on the predicted intensity pattern from theoretical calculations previously reported by Murray et al.<sup>35</sup> Close inspection of the pXRD pattern is required to identify the true phase. It is

concluded that the reported pseudo-ZB phase is likely a stacking-fault-rich WZ phase and may represent a phase in transition from the ZB to WZ structure as would be expected from Ostwald's Rule of Stages. While the TEM images of all pseudo-ZB samples clearly show stacking faults (Figures SI-6 and SI-9), the presence of stacking faults alone in the QD does not prove an intermediate phase.

**Evidence of an Intermediate Phase.** Ostwald's Rule of Stages predicts that the initially formed nuclei for a crystal growing from dissolved monomers should occur in the kinetic rather than the thermodynamic structure. The prediction is based upon the fact that the lowest energy packing of the fewest possible atoms is in the kinetic structure for a small crystallite. In the case of CdSe this would be the ZB phase. Following from Ostwald's predictions, the CdSe is expected to nucleate as a ZB crystal and convert to the thermodynamic phase potentially through an intermediate phase. The nature of the transformation may arise due to stacking fault migration appearing as a second-order phase transition or as a first-order melting phase transition where the  $T_M$  is proportional to the defect density in the growing crystal. It is anticipated that the pseudo-ZB phase boundary may represent such an intermediate phase during growth or a material where the rate of growth favors a high defect density. The intermediate phase may be anticipated to be unstable to stacking fault migration upon annealing of the crystallite lattice at elevated temperatures through a phase transition associated with lattice melting or during a long thermal annealing step if the Rule of Stages is involved. Although stacking faults are observed by TEM and pXRD, the stacking fault order or stacking fault density is not easily extracted from TEM or pXRD due to the number of TEM images required for accurate accounting and the ensemble nature of pXRD which cannot provide a direct measure of the stochastic stacking fault density. A more effective probe is the time- and temperature-dependent response of a solution or powdered pseudo-ZB sample analyzed using pXRD.

In Figure 4, the time-dependent change in the pXRD pattern for a 5.0 nm pseudo-ZB QD following solvothermal heating in HDA at 220 °C for 24 h is shown. The powder pattern appears to convert from ZB to WZ without a change in the QD size. The structural transformation in the pseudo-ZB structure is clearly demonstrated by the appearance of the (103) reflection coupled with a shift of  $\sim 3^\circ$  in the peak position at  $\sim 42^\circ$  due to transition from the ZB (110) to the WZ (220) reflection. The

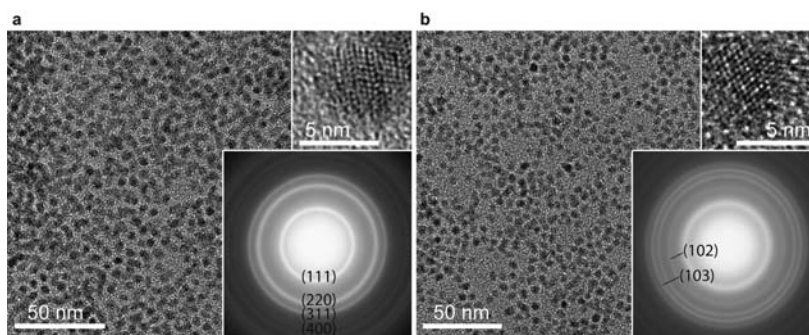


**Figure 3.** (A) TEM image of ZB (cubic) 5.2 nm CdSe (sample i), with insets showing (top) high-resolution TEM image of a typical nanocrystal and (bottom) the SAED pattern indexed to the cubic phase. (B) TEM image of WZ (hexagonal) 5.0 nm CdSe (sample vi), with insets showing (top) high-resolution TEM image of a typical nanocrystal and (bottom) the SAED pattern, with (102) and (103) diffraction rings being characteristic of the hexagonal phase. Size dispersity is presented in the Figure SI-8.

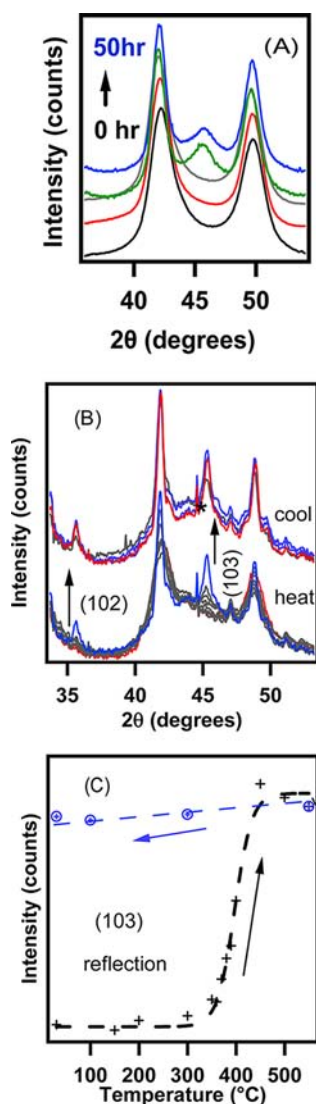


**Figure 4.** (A) Solvothermal annealing of pseudo-ZB CdSe (5.0 nm) in HDA at 220 °C. (B) Temperature-dependent pXRD on a powdered sample of ZB CdSe QDs (5.0 nm). (C) Plot of the temperature-dependent (103) reflection for ZB CdSe QDs (5.0 nm).

observed behavior is analogous to reported observations for the pXRD pattern of <3.0 nm CdSe QDs grown under lyothermal conditions, where the pattern change is attributed to the presence of stacking faults that anneal as the QD grows.<sup>36</sup>

No structural change in the pXRD pattern for QDs isolated in the ZB or WZ regions of the binary phase diagram occurs during post-synthesis annealing under solvothermal conditions, as would be anticipated for defect-free CdSe QDs. However, consistent with the anticipated phase transition to the thermodynamic phase predicted by Ostwald's Rule of Stages, a powdered sample of the pure ZB structure is anticipated to exhibit a first-order phase transition to the thermodynamic WZ structure. Inspection of the temperature-dependent pXRD data carried out on a powdered sample of 5.0 nm CdSe QDs exhibiting the ZB structure shows a well-defined first-order melting phase transition as the temperature is increased with complete conversion to a WZ indexable phase (Figure 4B). No structural relaxation is observed upon cooling as expected for a melting transition accompanied by relaxation into the thermodynamically stable phase. The plot of the intensity of

the (103) peak in Figure 4C, characteristic of WZ, as a function of temperature allows the melting transition to be assigned at ~400 °C. The phase transition is accompanied by a narrowing of the pXRD line width due to the melting transition leading to the onset of nanocrystal fusion following thermally induced ligand loss above 250 °C. The measured melting transition temperature for ZB→WZ is ~440 °C in thin films for CdSe phase transformation.<sup>37</sup>

**Insight into Phase Behavior.** The observation of an isolable stable kinetic and thermodynamic phase can be understood by considering the mechanism of crystal growth as described by nucleation theory and Ostwald's rules for crystallization, including Ostwald's Rule of Stages for crystal growth following initial nucleation. Coupling Ostwald's rules to nucleation theory, which predicts the critical nuclei form at the point where growth exceeds dissolution rates, the kinetics of the reaction should become important. At high monomer addition rates, one anticipates a higher defect error in atom arrangement at the growing crystal front and vice versa for low monomer addition rates. The lower defect density at low monomer addition rates would suppress the inter-conversion from ZB to WZ in CdSe. In fact, in Molecular Beam Epitaxially grown materials the ability to isolate ZB or WZ has been attributed to the defect density and film growth rates.<sup>26</sup>

The number of CdSe QDs in the reaction over time and the rate of growth for the three phase regimes observed are shown in Figure 5. At low monomer concentration, the linear rate of QD growth after 100 s follows the observed reduction in CdSe QD concentration, as anticipated for an Ostwald growth mechanism. In addition, the growth to the final QD size is slow. At high monomer concentration, the growth is nearly flat, indicating the growth to the final QD size is rapid. The intermediate regime exhibits a mixture of the two extremes. Inspection of the absorption profiles also is instructive. The low monomer controlled growth remains sharp throughout the growth, while the high monomer exhibits a broadened spectral profile.

The results of the kinetic traces suggest the observed phase boundaries may be influenced by rates of the monomer addition to the growing crystallite facets. At high monomer concentrations, the WZ phase is observed over all crystallite sizes due to the suppressed ZB→WZ phase transition temperature if high packing errors exist in the crystal, reflecting the rapid rate of monomer addition to the growing crystal. A high packing error density will lower the energy barrier for lattice relaxation. The observation of the ZB structure to >20 nm is believed to be due to the low ion packing errors in the growing crystallite due to slow monomer addition. The lower error density will raise the transition point, as a critical temperature must be reached to induce lattice melting. The pseudo-ZB regime represents an intermediate phase wherein the inter-conversion ZB→WZ may reflect an intermediate phase, as predicted by Ostwald's Rule of Stages. The results imply that the rationale for the typical observation of routine WZ phase isolation for CdSe QDs grown under high-temperature lyothermal conditions reflects the ease with which stacking faults form due to the rapid ion addition to the nanocrystal facets at the high monomer concentrations used in lyothermal reactions.

In the tetrapod structures for CdSe, formation of a cubic core followed by rapid arm growth in the WZ structure is consistent with the observations herein and indicates such structures are kinetically driven. Furthermore, the data would explain the

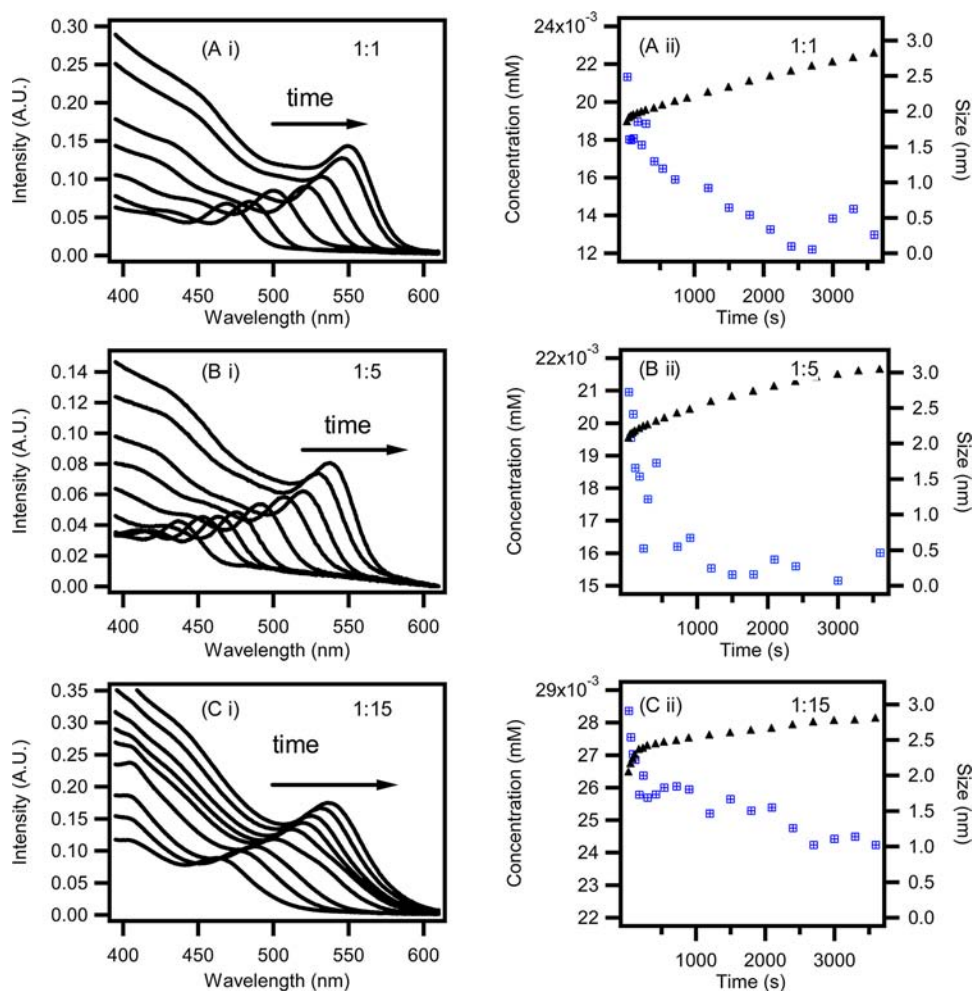


**Figure 5.** Changes in (i) UV-vis absorption spectra and (ii) QD size and concentration at a reaction carried out at 170 °C for (A) 1:1 Cd:Se mole ratio (10 mM CdSA), (B) 1:5 Cd:Se mole ratio (10 mM CdSA), and (C) 1:15 Cd:Se mole ratio (40 mM CdSA).

earlier observation of ligand control due to either a reduction in monomer accessibility and therefore the rate of ion addition or a change in the nanocrystal surface free energy due to passivation effects. These results would explain the observation that the passivant choice can allow selective structure isolation since the presence of the passivant does influence the monomer reactivity and ion addition rate during a lyothermal reaction.

## CONCLUSION

While previous studies have suggested that targeted isolation of the ZB phase requires the addition of alkyl phosphonic acids or other additives to direct formation of the desired structure, the results of the study reported herein indicate that, through Ostwald's Rule of Stages, the ZB structure is initially nucleated in the reaction and therefore can be maintained or converted to WZ under the correct reaction conditions, as plotted in the phase diagram. The ability to isolate a desired structural phase regardless of size confirms that no structural directing ligand is required; rather, only the principles of crystal nucleation formulated nearly two centuries ago dictate the isolated phase. The experimental results support a model wherein the critical nuclei are formed in ZB, the kinetic phase, and transforms to WZ, the thermodynamic phase, in accordance with Ostwald's observations in 1897.<sup>3</sup> The observation of a stable ZB phase grown at low monomer concentration, once nucleated, strongly implies that nucleation occurs in the ZB QDs and grows

epitaxially under conditions where few vacancies are present. Growth of the QDs appears to follow the simple rules of nucleation theory and the Rule of Stages, in which the structure at the point of nucleation is due to the surface free energy ( $\Delta G(p, T, \gamma)$ ) for the smallest crystal unit. Under slow growth conditions observed for low monomer concentrations in the reaction, few defects are believed to form within the growing QDs, and the addition of Cd and Se ions to the growing QD facet appears to occur in an epitaxial fashion. The result of the growth behavior is to maintain the initially formed phase until the surface energy of the phase exceeds the energy for phase transformation. It has been speculated previously that such growth behavior may represent the underlying mechanism for arm growth in tetrapod structures.<sup>24</sup> Under growth conditions at high monomer concentration conditions, ion addition is uncontrolled, resulting in stacking faults that lower the threshold for a melting transition, inducing a structural relaxation to the thermodynamic WZ phase. The interplay of growth rates, defect densities, and phase transformation corroborates the expectation from Ostwald's Rule of Stages.

## ASSOCIATED CONTENT

### Supporting Information

pXRD, TEM, and TEM-SAED images for the ZB, WZ, and pseudo-ZB CdSe QDs. This material is available free of charge via the Internet at <http://pubs.acs.org>.

## ■ AUTHOR INFORMATION

## Corresponding Author

strouse@chem.fsu.edu

## Present Address

<sup>§</sup>Industrial Research Limited, P.O. Box 31-310, Lower Hutt 5040, New Zealand

## Notes

The authors declare no competing financial interest.

## ■ ACKNOWLEDGMENTS

This work was supported by NSF under NSF-CHE 0911080, and the Florida-Georgia Lewis Stokes Alliance for Minority Participation fellowship (A.L.W.). R.D.T. thanks the MacDiarmid Institute and the Foundation for Research, Science and Technology (FRST) for funding through grant PROJ-13733-NMTS. S.C. thanks the FRST for funding through contract CONT-20707-NMTS-IRL.

## ■ REFERENCES

- (1) Gilbert, B.; Zhang, H.; Huang, F.; Banfield, J. F.; Ren, Y.; Haskel, D.; Lang, J. C.; Srajer, G.; Jugensen, A.; Zaychunas, G. A. *J. Chem. Phys.* **2004**, *120*, 11785–11795.
- (2) Bryan, J. D.; Gamelin, D. R. *Progress in Inorganic Chemistry*; 2005; Vol. 54.
- (3) Ostwald, W. Z. *Phys. Chem.* **1897**, *22*, 289–330.
- (4) Rengarajan, G. T.; Enke, D.; Steinhart, M.; Beiner, M. *Phys. Chem. Chem. Phys.* **2011**, *13*, 21367–21374.
- (5) Rein, P.; Frenkel, D. *Phys. Chem. Chem. Phys.* **1999**, *1*, 2191–2196.
- (6) Chung, S. Y.; Kim, Y. M.; Kim, J. G.; Kim, Y. J. *Nat. Phys.* **2009**, *5*, 68–74.
- (7) Erk, C.; Rohner, C.; Schlecht, S. Z. *Anorg. Allg. Chem.* **2008**, *634*, 3001–3004.
- (8) Navrotsky, A. *Proc. Natl. Acad. Sci. U.S.A.* **2004**, *101*, 12096–12101.
- (9) McHale, J. M.; Aurouz, A.; Perotta, A. J.; Navrotsky, A. *Science* **1997**, *277*, 788–791.
- (10) Gilbert, B.; Zhang, H.; Huang, F.; Finnegan, M. P.; Waychunas, G. A.; Banfield, J. F. *Geochem. Trans.* **2003**, *4*, 20–27.
- (11) Bandaranayake, R. J.; Wen, G. W.; Lin, J. Y.; Jiang, H. X.; Sorensen, C. M. *Appl. Phys. Lett.* **1995**, *67*, 831–833.
- (12) Peng, X. G.; Wickham, J.; Alivisatos, A. P. *J. Am. Chem. Soc.* **1998**, *120*, 5343–5344.
- (13) Dagtepe, P.; Chikan, V. J. *Phys. Chem. C* **2010**, *114*, 16263–16269.
- (14) Tsukimura, K.; Suzuki, M.; Suszaki, Y.; Murakami, T. *Cryst. Growth Design* **2010**, *10*, 3596–3607.
- (15) Smith, A. M.; Nie, S. M. *Acc. Chem. Res.* **2010**, *43*, 190–200.
- (16) Gao, X. H.; Cui, Y. Y.; Levenson, R. M.; Chung, L. W. K.; Nie, S. M. *Nat. Biotechnol.* **2004**, *22*, 969–976.
- (17) Klostranec, J. M.; Chan, W. C. W. *Adv. Mater.* **2006**, *18*, 1953–1964.
- (18) Sapsford, K. E.; Pons, T.; Medintz, I. L.; Mattoussi, H. *Sensors* **2006**, *6*, 925–953.
- (19) Murray, C. B.; Kagan, C. R.; Bawendi, B. G. *Science* **1995**, *270*, 1335–1338.
- (20) Wadia, C.; Alivisatos, A. P.; Kammen, D. M. *Environ. Sci. Technol.* **2009**, *43*, 2072–2077.
- (21) Shiohara, A.; Hanada, S.; Prabakar, S.; Fujioka, K.; Lim, T. H.; Yamamoto, K.; Northcote, P. T.; Tilley, R. D. *J. Am. Chem. Soc.* **2010**, *132*, 248–253.
- (22) Lita, A.; Washington, A. L., II; van de Burgt, L.; Strouse, G. F.; Stiegman, A. E. *Adv. Mater.* **2010**, *22*, 3987–2991.
- (23) Milliron, D. J.; Hughes, S. M.; Cui, Y.; Manna, L.; Li, J.; Wang, L. W.; Alivisatos, A. P. *Nature* **2004**, *430*, 190–195.
- (24) Ivanov, S. A.; Pirgatsinski, A.; Nanda, J.; Tretiak, S.; Zavadil, K. R.; Wallace, W. O.; Werder, D.; Klimov, V. I. *J. Am. Chem. Soc.* **2007**, *129*, 11708–11719.
- (25) Erwin, S. C.; Zu, L.; Haftel, M. I.; Efros, A. L.; Kennedy, T. A.; Norris, D. J. *Nature* **2005**, *436*, 91–94.
- (26) Pawar, S. M.; Pawar, B. S.; Kim, J. H.; Joo, O. S.; Lokhande, C. D. *Curr. Appl. Phys.* **2011**, *11*, 117–161.
- (27) Scher, E. C.; Manna, L.; Alivisatos, A. P. *Phil. Trans. R. Soc. London A* **2003**, *361*, 241–257.
- (28) Cao, Y. C.; Wang, J. J. *J. Am. Chem. Soc.* **2004**, *126*, 14336–14337.
- (29) Sun, B. Q.; Greenham, N. C. *Phys. Chem. Chem. Phys.* **2006**, *8*, 3557–3560.
- (30) Mohamed, M. B.; Tonti, D.; Al-Salman, A.; Chemseddine, A.; Chergui, M. J. *Phys. Chem. B* **2005**, *109*, 10533–10537.
- (31) Washington, A. L., II; Strouse, G. F. *Chem. Mater.* **2009**, *21*, 2770–2776.
- (32) Lovingood, D. D.; Oyler, R. E.; Strouse, G. F. *J. Am. Chem. Soc.* **2008**, *130*, 17004–17011.
- (33) Washington, A. L., II; Strouse, G. F. *Chem. Mater.* **2009**, *21*, 3586–3592.
- (34) Yu, W. W.; Qu, L.; Guo, W.; Peng, X. G. *Chem. Mater.* **2003**, *15*, 2854–2860.
- (35) Murray, C. B.; Norris, D. J.; Bawendi, B. G. *J. Am. Chem. Soc.* **1993**, *115*, 8706–8715.
- (36) Bawendi, M. G.; Kortan, A. R.; Steigerwald, M. L.; Brus, L. E. *J. Chem. Phys.* **1989**, *91*, 7282–7290.
- (37) Ju, Z. G.; Lu, Y. M.; Shan, C. X.; Zhang, J. Y.; Yao, B.; Shen, D. Z. *J. Phys. D: Appl. Phys.* **2008**, *41*, 015304.